Structural Determinants of the Stretching Frequency of CO Bound to Myoglobin[†,‡]

Tiansheng Li, Michael L. Quillin,[§] George N. Phillips, Jr., and John S. Olson*

Department of Biochemistry and Cell Biology and the W. M. Keck Center for Computational Biology, Rice University, Houston, Texas 77251-1892

Received August 23, 1993; Revised Manuscript Received November 24, 1993[⊗]

ABSTRACT: In order to assess the relative importance of polar *versus* steric interactions, infrared spectra and overall CO binding properties were measured at room temperature for 41 different recombinant myoglobins containing mutations at His[64](E7), Val[68](E11), Phe[43](CD1), Arg[45](CD3), Phe[46](CD4), and Leu[29](B10). The results were compared to the crystal structures of wild-type, Phe[29], Val[46], Ala[68], Phe[68], Gln[64], Leu[64], and Gly[64] sperm whale CO–myoglobin and that of Thr[68] pig CO–myoglobin. As observed in several previous studies, replacement of the distal histidine (His[64]) with aliphatic amino acids results in the appearance of a single IR band in the 1960–1970-cm^{-1} region and in large increases in CO affinity (K_{CO}). More complex behavior is observed for Gly, Ala, Gln, Met, and Trp substitutions at position 64, but in each case there is a net increase in the intensity of this high-frequency component. Replacement of Val[68] with Ala, Leu, Ile, and Phe produces little effect on the IR spectrum, whereas these mutations cause 20-fold changes in K_{CO}, presumably due to steric effects. Replacement of Val[68] with Thr decreases K_{CO} 4–5-fold, whereas the position of the major IR band increases from 1945 to 1961 cm^{-1}. Replacement of Val[68] with Asn also causes a large decrease in K_{CO}, but in this case, the peak position of the major IR band decreases from 1945 to 1916 cm^{-1}. Nine replacements were made in the CD corner at positions 43, 45, and 46. All of the resultant mutants show increased stretching frequencies that can be correlated with movement of the imidazole side chain of His[64] away from the bound ligand. All five substitutions at position 29 cause changes in the IR spectra. The Leu[29]→Phe mutation had the largest effect, producing a single band centered at 1932 cm^{-1}. Together these data demonstrate that there is little direct correlation between affinity, ν_{CO}, and Fe–C–O geometry. The major factor governing ν_{CO} appears to be the electrostatic potential surrounding the bound ligand and not steric hindrance. The presence of positive charges from proton donors, such as N_ϵ of His[64] and N_δ of Asn[68], causes a decrease in the bond order and stretching frequency of bound CO. In contrast, the negative portion of the Thr[68] dipole points directly toward the bound ligand and increases the C–O bond order and stretching frequency. Movement of His[64] away from the bound ligand or replacement of this residue with aliphatic amino acids prevents hydrogen-bonding interactions, causing ν_{CO} to increase. Placement of the positive portion of the aromatic multipole of Phe[29] next to bound CO has the opposite effect, causing a decrease in the order of the C–O bond. Substitutions that increase the space available in the distal pocket cause more subtle alterations in the IR spectrum, which can be attributed to increased conformational flexibility and enhanced polar interactions of the bound ligand with solvent water molecules. Thus, the vibrational spectrum of bound CO is a sensitive gauge of electrostatic potentials near the ligand binding site in myoglobin.

Studies of the binding of carbon monoxide to hemoproteins and heme model compounds have a long and rich scientific history. In general, CO binds to simple reduced heme complexes with a 1000-fold higher affinity than oxygen. If this relative affinity were maintained in mammalian myoglobins and hemoglobins, these proteins would become inactivated by the carbon monoxide that is produced endogenously for neurotransmission, blood pressure regulation, and hemin catabolism (Marks et al., 1991; Snyder & Brecht, 1992). Consequently, globins have evolved distal pocket structures that discriminate against CO in favor of O_2 binding. As a result of the physiological importance of this discrimination, much effort has been made to elucidate the structural mechanisms used by the proteins to inhibit CO binding.

Caughey and co-workers were among the first to show that the infrared stretching frequency of bound CO is a sensitive probe of the distal pocket structure in hemoglobins and myoglobins (Alben & Caughey, 1968; Caughey et al., 1969). These workers showed that the IR spectrum varies significantly with pH, temperature, and the structures of the amino acids directly adjacent to the bound ligand (Caughey et al., 1969; Choc & Caughey, 1981; Shimada & Caughey, 1982). In mammalian myoglobins, at least four different CO conformers can be identified in IR spectra and are currently designated A (for ground states), with subscripts numbered in descending order of their stretching vibration frequencies, i.e., 1965 (A_0), 1949 (A_1), 1942 (A_2), and 1932 (A_3) cm^{-1} (Caughey et al., 1969; Makinen et al., 1979; Caughey et al., 1981; Ansari et al., 1987; Frauenfelder et al., 1988). Under physiological conditions, the major conformers of mammalian myoglobins are a mixture of components A_1 and A_2 with $\nu_{1,2}$ = 1945 cm^{-1} (70%) and A_3 with ν_3 = 1932 cm^{-1} (30%). Acidification to pH values of <5.0 leads to the conversion of most of the absorbance intensity to the A_0 (1965 cm^{-1}) conformer, presumably as a result of increased protonation of the distal histidine (Shimada & Caughey, 1982; Ormos et al., 1988;

[†] Supported by United States Public Health Service Grants GM-35649, AR-40252, and HL-47020, by Grants C-612 and C-1142 from the Robert A. Welch Foundation, and by the W. M. Keck Foundation.

[‡] Coordinates and structure factors have been deposited in the Brookhaven Protein Data Bank under filenames 1SPL and 1MYM for Phe[29] and Val[46] CO–myoglobins, respectively.

[§] Recipient of graduate fellowships from the National Science Foundation and National Institutes of Health Training Grant GM-08280.

[⊗] Abstract published in *Advance ACS Abstracts,* February 1, 1994.

0006-2960/94/0433-1433$04.50/0

Ramsden & Spiro, 1989; Morikis et al., 1989). The A_0 conformer also is formed in significant amounts at cryogenic temperatures, even for native or wild-type myoglobins at pH 7.0 (Balasubramanian et al., 1993; Braunstein et al., 1993).

Correlation of the IR spectral species with specific structural features in the CO complexes has proved elusive. The textbook explanation for reduced CO affinity in sperm whale myoglobin is unfavorable interactions between the distal histidine (E7) and the bound ligand (Stryer, 1988). This steric hindrance is postulated to prevent the formation of a linear Fe–C–O geometry, which is the preferred orientation in sterically unhindered model compounds, and the resulting bent geometry would decrease the order of the C–O bond due to the requirement of sp^2 hybridization of the carbon atom (Peng & Ibers, 1976; Collman, 1976). Two bent Fe–C–O conformations (θ = 141 and 120°) were reported in the high-resolution crystal structure of native sperm whale CO–myoglobin (Kuriyan et al., 1986). Initial mutagenesis experiments with sperm whale myoglobin showed that the His^{64}(E7)→Gly mutation causes a marked increase in CO affinity and the appearance of a broad and complex IR band centered at 1964 cm^{-1}. Both of the latter effects were attributed to the relief of steric hindrance by removal of the large imidazole side chain. More direct correlation between CO stretching vibrations and Fe–C–O bond angles has also been reported (Ormos et al., 1988; Nagai et al., 1991). However, subsequent studies with a larger set of mutants have indicated that polarity may play a more significant role in regulating CO affinity and stretching frequency than steric effects (Springer et al., 1989; Rohlfs et al., 1990; Smerdon et al., 1991; Lian et al., 1993).

Infrared and resonance Raman studies of the carbon monoxide complexes of a wide variety of heme proteins and model compounds have shown that the stretching frequency of the C—O bond is inversely correlated with that for the Fe—C bond (Uno et al., 1985; Li & Spiro, 1988; Nagai et al., 1991). Li and Spiro (1988) have interpreted this inverse correlation between ν_{CO} and ν_{FeC} in terms of back bond donation from the iron atom. They suggested that proton donors adjacent to the O atom of the bound ligand enhance the degree of back-bonding, increasing the order of the Fe–C bond and decreasing the order of the C—O bond due to the formation of $Fe^{\delta(+)}{=}C{=}O^{\delta(-)}$ resonance structures. The presence of negative electrostatic potentials next to the oxygen atom would have the opposite effect, increasing the order of the C—O bond and forming $Fe^{\delta(-)}{-}C{\equiv}O^{\delta(+)}$ resonance structures. Building on this idea, Oldfield and co-workers have proposed that tautomerism of distal histidine, coupled with movements of the imidazole ring away from the bound ligand, can account for the chemical shifts and stretching frequencies of all four CO conformers in native myoglobin (Oldfield et al., 1991; Park et al., 1991).

Four very recent publications have provided more support for the theory that polarity plays the key role in governing the stretching frequency of bound carbon monoxide. First, the angle for the Fe–C–O complex is 169° in the *P6* crystal form of wild-type sperm whale myoglobin and does not change significantly when His^{64} is replaced by either Gly, Gln, or Leu, even though the mutations all cause significant increases in CO affinity and ν_{CO} (Quillin et al., 1993). Second, Cameron et al. (1993) have shown that the Fe–C–O angle is also 160–170° in the Val^{68}→Thr mutant of pig myoglobin. In contrast to the position 64 mutations, this isosteric substitution causes a marked decrease in K_{CO}, despite the appearance of a major IR band at 1961 cm^{-1}. The increase in ν_{CO} was interpreted in terms of an interaction between the bound ligand and the partial negative charge on the Thr^{68} hydroxyl. Third, Ray et al. (1993) showed that polar interactions with the superstructure of capped model hemes, and not distortion due to steric hindrance, caused the large variations in ν_{CO} and ν_{FeC} observed for these compounds. Fourth, Balasubramanian et al. (1993) reported that replacement of Val^{68} with Asn in human myoglobin causes the appearance of a major band at 1915 cm^{-1} in the IR spectrum of the mutant CO complex at room temperature. They offered an explanation in terms of steric hindrance since the association rate constant for CO binding to this mutant was ~10-fold less than that of wild-type human myoglobin. However, it is also possible that protons from the N_δ atom of the Asn side chain are interacting electrostatically with bound CO.

These recent publications and the theoretical work of Li and Spiro (1988) and Park et al. (1991) motivated us to measure the infrared spectra and CO binding properties of 41 recombinant sperm whale and pig myoglobins. Mutations at key positions in the distal pocket were selected in order to systematically change the electrostatic potential adjacent to the bound ligand. Substitutions were also made in the CD corner in an attempt to change the orientation of the imidazole side chain of His^{64}. The spectral and functional results have been compared to wild-type, six previously determined, and two new mutant crystal structures of CO–myoglobin in an effort to look for correlations between Fe–C–O geometry, ν_{CO}, and ligand affinity.

EXPERIMENTAL PROCEDURES

Site-Directed Mutagenesis. The preparation of site-directed mutants of sperm whale myoglobin has been described by Springer et al. (1989), Egeberg et al. (1990a,b), and Carver et al. (1992). For most of the new mutants, the *Pst*I–*Kpn*I fragment of pMb413a containing the synthetic sperm whale myoglobin constructed by Springer and Sligar (1987) was subcloned into pEMBL19 for mutagenesis, sequencing, and expression. The resultant vector has been designated pEMbS-1 (Carver et al., 1992). All DNA manipulations were performed as described by Sambrook et al. (1989). The Kunkel method of oligonucleotide-directed mutagenesis was used for new substitutions at positions 29, 43, 45 and 46 (Kunkel et al., 1985). New mutants at positions 64 and 68 were constructed by cassette mutagenesis, often using the original pMb413a plasmid (Springer et al., 1989; Egeberg et al., 1990a,b). The vectors harboring the Mb genes were transformed into *Escherichia coli* strain TB1 and expressed constitutively as described by Springer and Sligar (1987). The 100-L fermentation facility at Rice University was used to obtain 400–500 g of packed cells containing soluble holoprotein. The purification scheme was described previously (Springer & Sligar, 1987; Carver et al., 1992). Wild-type, Val^{64}, Thr^{68}, Ser^{68}, and Val^{64}–Thr^{68} pig myoglobins were expressed and purified starting with plasmids provided by Anthony J. Wilkinson from York University (Smerdon et al., 1991; Cameron et al., 1993).

Kinetic Measurements. Association and dissociation rate constants for CO binding were measured using a stopped-flow, rapid mixing technique as described by Rohlfs et al. (1990). The association rate constants were obtained by analyzing time courses for the reaction the deoxy forms of the proteins with at least three different concentrations of CO in 0.1 M phosphate/1 mM EDTA (pH 7.0) at 20 °C. The dissociation rate constants were obtained by analyzing time

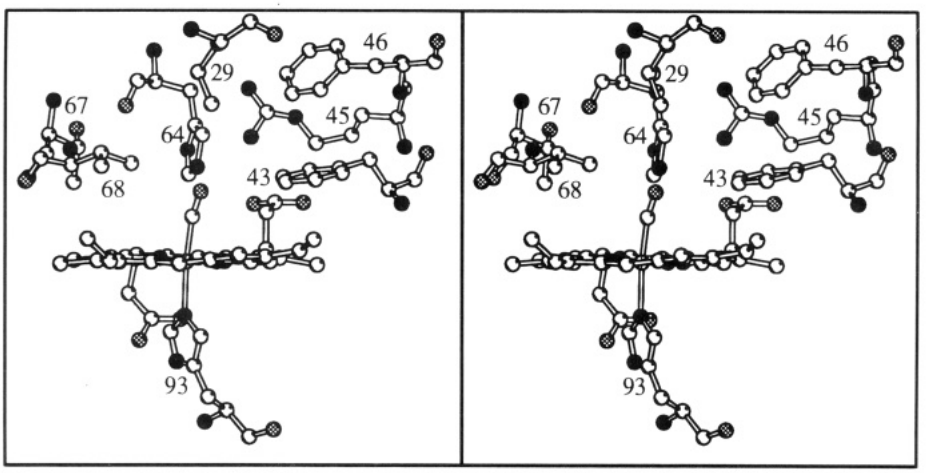

FIGURE 1: Stereoview of the distal pocket of wild-type sperm whale CO–myoglobin. The view is from a position near the back of the distal pocket (Ile^{107}) looking out toward the solvent. The coordinates were taken from Quillin et al. (1993). The sites of amino acid substitutions described in this study are labeled with their respective sequence numbers. Carbon atoms are represented by open circles, oxygen atoms by shaded circles, and nitrogen atoms by filled circles. The drawing was made with the program MOLSCRIPT (Kraulis, 1991).

courses for the displacement of CO by high concentrations of NO under the same buffer conditions (Rohlfs et al., 1990). Briefly, deoxymyoglobin was passed through a Sephadex G-25 column equilibrated with 0.1 M phosphate/1 mM EDTA (pH 7.0) buffer under 1 atm of CO, and the eluant containing CO–myoglobin was diluted into the phosphate buffer purged with 1 atm of nitrogen gas. The solution containing CO–myoglobin was rapidly mixed with the phosphate buffer equilibrated with 1 atm of NO gas in a stopped-flow spectrometer, and the time course of CO replacement was recorded by following absorbance changes at 426 nm.

X-ray Crystallography. The structures of the oxy and aquomet forms of Phe^{29} have been reported by Carver et al. (1992), and the structures of the aquomet forms of Val^{46} and Leu^{46} have been determined by Lai and Phillips (H. Lai and G. N. Phillips, Jr., unpublished work). Structures of the CO complexes of the Val^{46} and Phe^{29} mutants were determined for this work. Crystals were grown in the *P*6 form using 2.6 M ammonium sulfate in Tris buffer at pH 9.0, as described by Phillips et al. (1990) and Quillin et al. (1993). The crystals were treated with 5 mg/mL sodium dithionite in the presence of 1 atm of carbon monoxide. Diffraction data for the mutant CO complexes were collected on either a Siemens X-1000 or an R-Axis IIC are detector equipped with a rotating anode source and processed using XDS (Kabash, 1988) or Rigaku supplied software. The number of unique reflections for the Phe^{29} and Val^{46} crystals was 15 363 and 23 681, respectively. Starting models for refinement of the mutant MbCO structures were generated from the corresponding metmyoglobin coordinates. Constrained least-squares refinement was accomplished with either PROFFT or X-PLOR programs using the PROLSQ parameter set (Finzel, 1987; Brunger et al., 1989). After several cycles of refinement, manual refitting, and solvent placement, the crystallographic *R* factors converged to the values 14.6% and 16.1%, respectively, for the Phe^{29} and Val^{46} MbCO structures. The final structures were determined to 1.7-Å resolution with 66.4% and 95.7% completeness for the Phe^{29} and Val^{46} data sets, respectively. The coordinates and structure factors for these two mutant carbon monoxide myoglobins have been deposited with the Brookhaven Protein Data Bank, from which copies are available under the access codes 1SPL and 1MYM for Phe^{29} and Val^{46} CO–myoglobins, respectively.

FTIR Spectroscopy. Samples of MbCO were prepared as follows. A small amount of solid dithionite was added to a concentrated stock solution of the appropriate myoglobin to reduce the iron atom and remove molecular oxygen. The resultant deoxymyoglobin solution was eluted from a Sephadex G-25 column with 0.1 M potassium phosphate/1 mM EDTA (pH 7.0) buffer equilibrated with 1 atm of CO gas. The sample was concentrated to 3–5 mM heme and then reequilibrated with pure CO gas. One or two grains of dithionite were added to remove any residual oxygen just prior to recording the vibrational spectrum. Approximately 30 μL of the MbCO solution was added slowly to the IR cuvette to obtain an uniform film. The cuvette consists of two CaF_2 windows separated by a 56-μm spacer and was purged with nitrogen gas immediately before the sample was added. Spectra were recorded at 2-cm^{-1} resolution in the region 1800–2100 cm^{-1} using a Mattson Galaxy 6020 spectrometer interfaced with a Compaq 386 computer. Up to 10 000 interferograms were collected for all samples and the corresponding buffer controls. The final IR spectra were corrected for buffer background by digitial subtraction of the sample and control data.

RESULTS

The distal pocket of wild-type sperm whale CO–myoglobin is shown in Figure 1. The relative importance of steric hindrance and polar interactions was investigated by mutating those residues (64, 68, 29, and 43) which are directly adjacent to the bound ligand. We chose not to introduce amino acids with unit charges at these positions on the basis of two previous observations. First, the side chains of Arg^{64} and Asp^{64} mutants appear to move out toward the solvent, creating an open distal pocket which exhibits spectral and functional properties similar to those of Gly^{64} and Ala^{64} myoglobins (Springer et al., 1989; Morikis et al., 1990). Second, the introduction of charged residues in the interior of the distal pocket results in either unstable proteins or hemichromes in which the side chain of the mutated residue is chelated directly to the iron atom (Perutz et al., 1972; Varadarajan et al., 1989a,b; Egeberg et al., 1990a,b). Replacements in the CD corner at positions 45 and 46 were constructed in order to investigate second-order effects that change the orientation of the His^{64} side chain.

Replacement of the Distal Histidine with Neutral Amino Acids. Vibrational spectra of a large number of E7 mutants of myoglobin and hemoglobin have been reported, and our results in Figure 2 serve to summarize and expand the previous data set to include the Trp^{64} mutant (Caughey et al., 1969; Morikis et al., 1989, 1990; Egeberg et al., 1990a,b; Nagai et

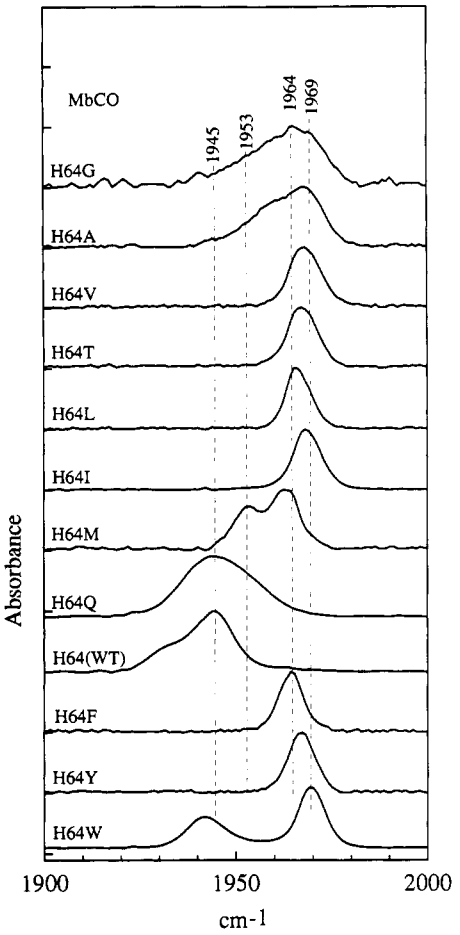

FIGURE 2: IR spectra of position 64 mutants of sperm whale CO–myoglobin measured at room temperature (~22 °C) in 0.1 M potassium phosphate/1 mM EDTA (pH 7.0). The mutant proteins are designated by a single letter abbreviation for the native residue, the position in the primary sequence, and the abbreviation for mutant amino acid, *viz.*, His^{64}→Gly is listed as H64G. WT stands for wild-type myoglobin. The spectra of the mutants are shifted to higher frequencies due to the loss of hydrogen-bonding interaction with His^{64}.

al., 1991; Sakan et al., 1993; Balasubramanian et al., 1993; Cameron et al., 1993). All of the position 64 mutants except Gln^{64} myoglobin show a maximum peak intensity above 1960 cm^{-1}, demonstrating that replacement of the distal histidine almost invariably results in conversion of the $A_{1,2}$ and A_3 states into the A_0 conformer.

The IR absorbance bands for Gly^{64} and Ala^{64} myoglobin are very broad with spectral band widths of 15–20 cm^{-1} and are consistent with previous observations for Gly^{64} CO–myoglobin by Morikis et al. (1989). The Fe–C band of Gly^{64} CO–myoglobin displays a similar large band width (~25 cm^{-1}) and clearly contains multiple spectral components. The two major components for the Fe–C stretch are at 492 and 506 cm^{-1} and are better resolved than the IR C–O bands (Morikis et al., 1989). The simplest explanation is that bound CO is exposed to solvent in these mutants. In some orientations and protein conformations, the water molecules will exert a positive electrostatic potential, decreasing ν_{CO}, and in others a negative potential, increasing ν_{CO}. The net result is substantial line broadening. The crystal structures of both the CO and aquomet forms of the Gly^{64} mutant show a wide open distal pocket containing solvent water molecules adjacent to the coordinated ligand (Quillin et al., 1993). The same exposure to solvent is thought to occur for Ala^{64} myoglobin, since the spectral properties of both the human and sperm whale mutants indicate that water is coordinated to the iron atom in the ferric state (Ikeda-Saito et al., 1992; Quillin et al., 1993).

The peak position for Gln^{64} CO–myoglobin is identical to that observed for the native protein. This suggests that similar polar and steric interactions occur between the bound ligand and the N_ϵ atom in both the imidazole and the propylamide side chains. However, the Gln^{64} band is very broad, and there is considerably more absorbance at frequencies greater than 1950 cm^{-1}. Again, the simplest explanation involves multiple protein–ligand conformations differing in the extent and polarity of electrostatic interactions. For example, two extreme two orientations of the side chain are possible with respect to electrostatic interactions: one in which protons from N_ϵ are adjacent to the bound CO, and a second in which the nonbonded electrons of the O_ϵ atom are next to the ligand. In addition, the Gln^{64} side chain does move away from the iron atom when CO is bound and is less well-defined than the imidazole side chain in wild-type myoglobin (Quillin et al., 1993).

Replacement of His^{64} with aliphatic amino acids produces a single narrow IR band in the 1960–1970-cm^{-1} range, regardless of size (Figure 2, Table 1). Despite the change in polarity, no differences were observed between the ligand binding and spectral properties of Val^{64} and Thr^{64} myoglobin, presumably because the Thr^{64} hydroxyl is too far away from the bound ligand to interact with it (Quillin et al., 1993). Phe^{64} and Tyr^{64} CO–myoglobins also exhibit narrow bands at ~1965 cm^{-1}. The results for these 64 mutants also demonstrate that there is little correlation between ν_{CO} and affinity. For example, K_{CO} for the Leu^{64} mutant is abnormally high, 1100 μM^{-1}, whereas that for the Tyr^{64} protein is very low, 5 μM^{-1}, and yet both proteins show a single stretching band centered at ~1965 cm^{-1}.

More complex behavior is observed for the Met^{64} and Trp^{64} mutants. The IR band for Met^{64} is broad and clearly composed of two distinct bands centered at 1953 and 1962 cm^{-1}. Rohlfs et al. (1990) reported biphasic time courses for oxygen and CO dissociation from this mutant that also suggest multiple conformations for the thioether side chain. Trp^{64} CO–myoglobin shows two well-separated bands centered at 1942 and 1969 cm^{-1}. Curiously, K_{CO} for this mutant is identical to that of native myoglobin, despite the large size of the indole side chain. It is difficult to interpret the origin of the two IR conformers without a structure, and unfortunately, we have had difficulty in crystallizing Trp^{64} myoglobin. It is possible that the indole NH group or the positive edge of the aromatic multipole of Trp^{64} may interact with the bound CO ligand to cause the appearance of the 1942-cm^{-1} band.

Polarity and Steric Hindrance at Residue 68(E11). The side chain of Val^{68} is very close to the heme iron atom and is thought to sterically hinder the binding of ligands (Figure 1). This idea is supported by the 2-fold increase in K_{CO} when Val^{68} is replaced by Ala (Table 1; Egeberg et al., 1990a,b). Substitution of Ile for Val^{68} places a C_δ atom almost directly over the iron and results in a 10-fold decrease in CO affinity (Egeberg et al., 1990a,b; unpublished structure of Ile^{68} metmyoglobin, M. L. Quillin and G. N. Phillips, Jr.). Intermediate changes in affinity are observed for the Leu^{68} and Phe^{68} mutants (Table 1). Despite these large changes in K_{CO} due to differing degrees of steric hindrance, the aliphatic and Phe substitutions at position 68 exert little effect on the vibrational spectrum of bound CO (Figure 3). The peak intensity is 1941–1945 cm^{-1} for Ala^{68}, Val^{68}(wild-type), Leu^{68}, Ile^{68}, and Phe^{68} myoglobins. There are changes in band width and shape, with the wild-type and Phe^{68} proteins showing significant amounts of the A_3 or 1932-cm^{-1} component and with Leu^{68}, Ile^{68}, and Gln^{68} showing relatively symmetric CO bands centered at 1941 cm^{-1}. However, these effects are quite

Table 1: IR Stretching Bands and Kinetic Parameters for Sperm Whale CO–Myoglobin Mutants at pH 7.0, 20–22 °C

protein	ν_0 (%)[a] (cm^{-1})	$\nu_{1,2}$ (%) (cm^{-1})	ν_3 (%) (cm^{-1})	$\bar{\nu}_{CO}$[b] (cm^{-1})	k'_{CO}[c] (μM^{-1} s^{-1})	k_{CO} (s^{-1})	K_{CO} (μM^{-1})
wild-type		1945 (70)	1932 (30)	1941	0.51	0.019	27
His64 mutants							
Gln^{64}		1945 (100)		1945	0.98	0.012	82
Gly^{64}	1965 (100)			1965	5.8	0.038	150
Ala^{64}	1966 (100)			1966	4.2	0.061	69
Val^{64}	1967 (100)			1967	7.0	0.048	150
Thr^{64}	1966 (100)			1966	6.9	0.045	150
Leu^{64}	1965 (100)			1965	26	0.024	1100
Ile^{64}	1968 (100)			1968	8.0	0.047	170
Met^{64}	1962 (58)	1953 (42)[d]		1958	4.6	0.023	200
Phe^{64}	1964 (100)			1964	4.5	0.054	83
Tyr^{64}	1966 (100)			1966	0.5	0.092	5.4
Trp^{64}	1969 (60)	1942 (40)		1958	0.65	0.023	28
Val^{68} mutants							
Ala^{68}		1945 (81)	1932(19)	1943	1.2	0.021	57
Ser^{68}	1963 (21)	1947 (69)	1932 (10)	1949	0.28	0.044	6.4
Leu^{68}		1941 (75)	1930 (25)	1938	0.53	0.011	48
Asn^{68}		1936 (30)[e]	1916 (70)[e]	1922	0.041	0.0096	4.3
Ile^{68}		1941 (70)	1930 (30)	1938	0.05	0.024	2.1
Gln^{68}	1963 (7)	1940 (65)	1932 (28)	1939	0.012	0.011	1.1
Phe^{68}		1945 (64)	1932 (36)	1940	0.25	0.018	14
Phe^{43} mutants							
Val^{43}	1967 (32)	1954 (68)		1958	0.36[f]	0.050[f]	7.2
Trp^{43}	1960 (100)			1960	0.23	0.045	5.1
Arg^{45} mutants							
Glu^{45}	1965 (19)	1946 (59)	1932 (22)	1946	0.32	0.042	7.6
Phe^{46} mutants							
Ala^{46}	1967 (79)	1950 (21)		1963	0.47	0.078	6.0
Val^{46}	1965 (80)	1950 (20)		1962	1.1	0.064	17
Leu^{46}	1965 (80)	1950 (20)		1962	0.50	0.056	8.9
Ile^{46}	1965 (63)	1948 (37)		1959	1.2	0.061	20
Tyr^{46}	1967 (6)	1945 (67)	1932 (27)	1943	0.43	0.027	16
Trp^{46}	1965 (10)	1947 (73)	1934 (17)	1947	0.28	0.032	8.8
Leu^{29} mutants							
Ala^{29}	1965 (6)	1947 (51)	1935 (43)	1943	0.26	0.019	14
Val^{29}	1965 (6)	1946 (43)	1933 (51)	1941	0.18	0.016	11
Ile^{29}	1965 (4)	1945 (48)	1932 (48)	1940	0.23	0.018	13
Phe^{29}			1932 (100)	1932	0.20	0.006[f]	33
Trp^{29}	1956 (37)	1945 (63)		1949	0.0039	0.008[f]	0.49
double mutants							
$Phe^{29}Leu^{64}$	1962 (100)			1962	6.7	0.018	370
$Phe^{29}Gln^{64}$		1950 (35)	1937 (65)	1942	0.51	0.006	85
$Phe^{29}Trp^{64}$	1964 (13)		1937 (87)	1941	0.52	0.007[f]	74

[a] The frequency of the IR band was determined by the peak position, with estimated experimental error ±1 cm^{-1}, and the intensity of the IR band was determined by the peak height and was normalized to the strongest band with estimated experimental error ±10%. [b] The value of ν_{CO} is a weighted measurement of the IR CO spectral components, as computed by $\nu_{CO} = \sum f_i \nu_i$, where f_i is the fraction of intensity measured by peak height, and ν_i is the peak frequency of spectral component i. [c] The estimated standard deviations for the measurements of rate constants k'_{CO}, k_{CO}, and K_{CO} were ±20% [d] The spectral component near 1950 cm^{-1} is tentatively classified as the A_1 conformer for comparison. [e] The spectral component near 1916 cm^{-1} is tentatively classified as the A_3 conformer, while that at 1936 cm^{-1} as A_1 for comparison with other mutants. [f] The time courses for CO binding to and release from these mutant CO–myoglobins are heterogeneous, and the parameters listed represent estimates based on fitting to a single exponential expression, even though the fits were poor. In the cases of the Phe^{29} and Trp^{29} mutants, simple behavior was observed in the association reactions but two phases were distinguishable in the NO replacement reactions as described by Carver et al. (1992).

small and on the same order of magnitude as the differences between wild-type sperm whale, human, and pig myoglobins (Figures 3 and 4; Balasubramanian et al., 1993).

Much larger changes in the IR spectrum are observed when polar residues are introduced into the 68 position. Substitution of Thr for Val^{68} in pig myoglobin produces a protein with a crystal structure which is isomorphous with that of the wild-type protein (Smerdon et al., 1990; Cameron et al., 1993). However, this mutation causes a dramatic shift in the IR band to 1961 cm^{-1} and a 4-fold decrease in CO affinity (Table 2, Figure 4; Cameron et al., 1993). High-resolution X-ray data for the pig mutant show that the Thr^{68} hydroxyl denotes a proton to the backbone carbonyl oxygen of His^{64} (Smerdon et al., 1990; Cameron et al., 1993). The nonbonded electrons on O_γ point toward the coordinated water in the aquomet structure, toward the non-coordinated water molecule, which is hydrogen-bonded to His^{64} in the deoxy structure, and toward the bound ligand in the CO structure. These observations led Cameron et al. (1993) to propose that the negative charge adjacent to bound CO causes the shift in intensity from the $A_{1,2}$ to the A_0 conformer. An 18-cm^{-1} increase was also seen when the Val^{68}→Thr mutation was introduced into Val^{64} pig myoglobin, resulting in a band centered at 1984 cm^{-1} (Figure 4, Table 2). Much smaller effects were observed for the Val^{68}→Ser mutation in either pig or sperm whale myoglobin, presumably because the hydroxyl group can rotate away from the bound ligand (Figures 3 and 4).

Replacement of Val^{68} with Asn in sperm whale myoglobin also produces a 7-fold decrease in K_{CO}, but in this case the maximum peak intensity in the IR spectrum decreases to 1916 cm^{-1} (Figure 3 and Table 1). Balasubramanian et al. (1993) observed the same result for Asn^{68} human CO–myoglobin and interpreted the shift in ν_{CO} and decrease in k'_{CO} in terms of steric hindrance. In the structure of Leu^{68} metmyoglobin, the isobutyl side chain is pointed toward the back of the distal pocket, away from the coordinated water molecule (M. L. Quillin and G. N. Phillips, Jr., unpublished results). One of the δ-CH_3 groups is located ~3.3 Å away from the position expected for the second atom of bound CO. If the side chain of Asn^{68} adopts a similar conformation, with the carbonyl

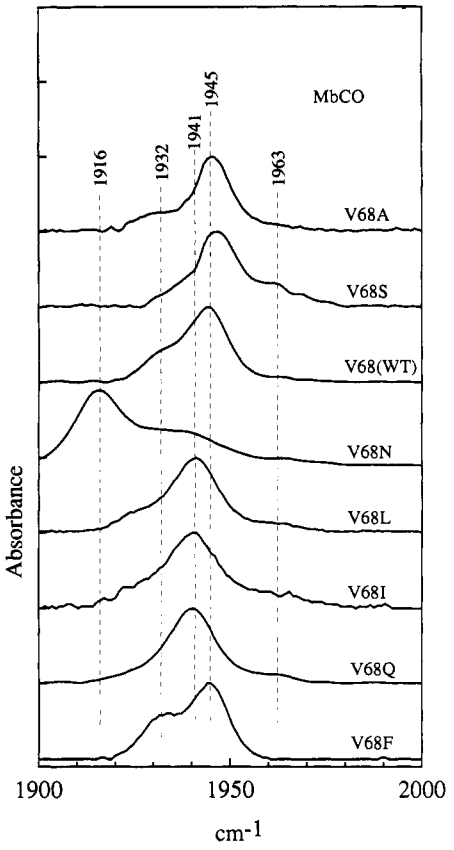

FIGURE 3: IR spectra of position 68 mutants of sperm whale CO–myoglobin measured at room temperature (~22 °C) in 0.1 M potassium phosphate/1 mM EDTA (pH 7.0). The polarity of the Asn[68] residue in the vicinity of the CO ligand causes a dramatic decrease in ν_{CO}.

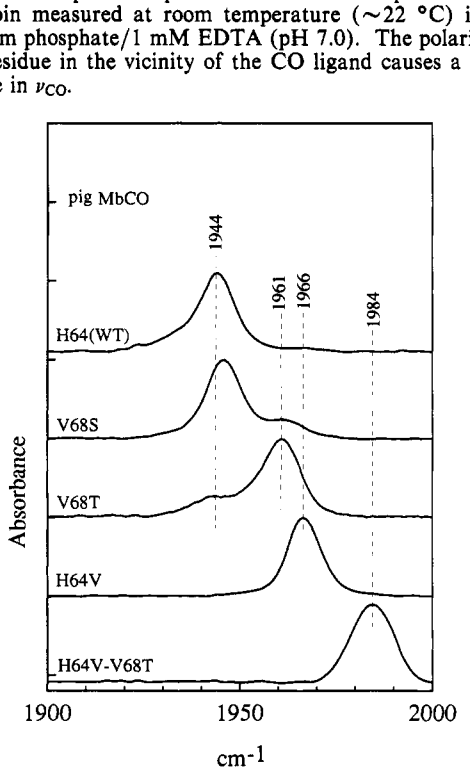

FIGURE 4: IR spectra of position 64 and 68 mutants of pig CO–myoglobin measured at room temperature (~22 °C) in 0.1 M potassium phosphate/1 mM EDTA (pH 7.0). The spectra for wild-type (WT), Val[64] (H64V), Thr[68] (V68T), and Val[64]Thr[68] (H64V–V68T) were taken from Cameron et al. (1993). The spectrum for Ser[68] (V68S) was measured for this work. The β-OH of the Thr[68] residue interacts with the CO ligand, causing a dramatic increase in ν_{CO}.

oxygen occupying the δ position farthest from the iron atom, the amide N_δ atom could be within hydrogen-bonding distance of the bound ligand. Such an interaction would account for the dramatic decrease in ν_{CO} produced by the Val[68]→Asn mutation. If N_δ and O_δ switched positions, the sign of the electrostatic potential near the bound ligand would change and cause ν_{CO} to increase. The existence of small populations of the latter and intermediate conformers would explain the extremely broad absorbance signal shown by the Asn[68] mutant.

The Val[68]→Gln mutation produces a dramatic 30-fold decrease in CO affinity, but almost no change in the IR spectrum of bound CO. This result again points out that there is little direct correlation between K_{CO} and ν_{CO}. The lack of change in the stretching frequency suggests that the amide portion of the Gln[68] side chain is located far away from the bound ligand. The decrease in affinity is probably due to further stabilization of distal pocket water molecules in deoxymyoglobin rather than to any direct electrostatic interactions, since the amide group is too far away from the bound CO to influence the IR spectrum. An exact interpretation will require a high-resolution crystal structure.

Substitutions at Position 29(B10). Both kinetic measurements and molecular dynamic simulations have shown that the physical size of residue 29 plays a major role in governing ligand rebinding following either photo- or thermal dissociation of the Fe–ligand bond (Adachi et al., 1992; Carver et al., 1992; Gibson et al., 1993; Li & Elber, 1993). Adachi et al. (1992) have shown that Leu[29]→Ala,Ile mutations cause an increase in intensity for the 1932-cm^{-1} (A_3) band of recombinant human CO–myoglobin. We have obtained the same result for Leu[29]→Ala, Val, and Ile substitutions in sperm whale myoglobin (Figure 5).

The Leu[29]→Phe mutation leads to a complete conversion to the A_3 or 1932-cm^{-1} band with little change in CO affinity. As shown in Figure 6, the Fe–C–O bond angle is slightly smaller in this mutant, and the ligand has rotated toward the nitrogen atom of the pyrrole A ring as a result of a small inward movement of the His[64] side chain. However, these changes in ϕ are observed in other mutants that exhibit high-frequency bands (Table 3). The most likely cause of the decrease in ν_{CO} is interaction of the bound ligand with the positive edge of the aromatic multipole of Phe[29]. The distance between the C_ζ carbon of the benzyl side chain and the oxygen atom of the bound CO is 3.0 Å, which is identical to the distance observed in the oxy complex of this mutant (Carver et al., 1992). This multipole interaction increases the O_2 affinity 15-fold, whereas a much smaller effect is observed for CO binding. Consistent with the increase in the Fe–C bond order, a more than 3-fold decrease in the rate of CO dissociation is observed (Table 1).

The strength and importance of this aromatic interaction were examined by introducing the Leu[29]→Phe mutation into proteins containing Leu, Gln, and Trp at position 64. The results for these double mutants are shown in Figure 7 and Table 1. In each case, a decrease in the position of the peak intensity of the IR spectrum is observed; however, the magnitude of the shift varied considerably. Only a 3-cm^{-1} decrease was observed for the Leu[64] protein, whereas most of the absorbance intensity for Trp[64] myoglobin shifted from 1970 to 1937 cm^{-1} when Leu[29] was replaced with Phe. An intermediate result was observed for the Gln[64] double myoglobin. For both Gln[64] and Trp[64] CO–myoglobins, the Leu[29]→Phe mutation leads to a decrease in k_{CO}, as was observed for the single Phe[29] mutant (Table 1).

In contrast to the other mutants in this series, the Leu[29]→Trp replacement causes a shift to higher frequencies in the IR spectrum. The intensity found at 1932 cm^{-1} for wild-type myoglobin is gone, and a significant band appears at 1955

Table 2: IR Stretching Bands and Kinetic Parameters for Pig CO–Myoglobin Mutants at pH 7.0, 20–22 °C

protein	ν_0 (%) (cm^{-1})	ν_1 (%) (cm^{-1})	ν_3 (%) (cm^{-1})	$\bar{\nu}_{CO}$ (cm^{-1})	k'_{CO}[a] (μM^{-1} s^{-1})	k_{CO} (s^{-1})	K_{CO} (μM^{-1})
pig wild-type[b] ($His^{64}Val^{68}$)	1965 (5)	1945 (70)	1932 (25)	1941	0.78	0.020	39
pig Ser^{68}	1961 (20)	1946 (80)		1949	1.1	0.044	25
pig Thr^{68} [b]	1961 (80)	1945 (20)		1958	0.60	0.080	7.5
pig Val^{64} [b]	1966 (100)			1966	6.4	0.05	130
pig $Val^{64}Thr^{68}$ [b]	1984 (100)			1984	27	0.063	430

[a] The estimated standard deviations for the measurements of rate constants k'_{CO}, k_{CO}, and K_{CO} were ±20%. [b] IR spectra and rate constants for these proteins were taken from Cameron et al. (1993).

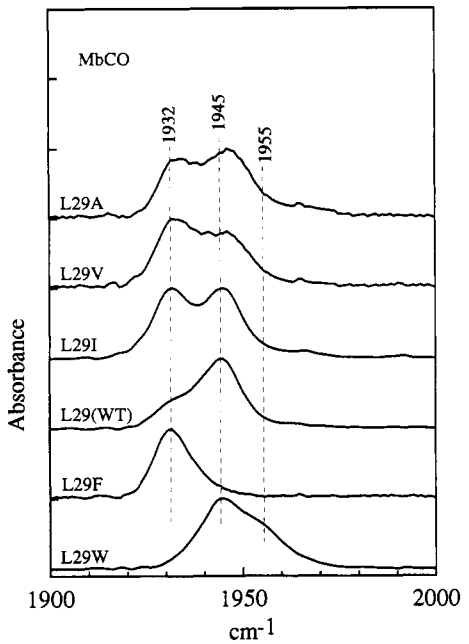

FIGURE 5: IR spectra of position 29 mutants of sperm whale CO–myoglobin measured at room temperature (~22 °C) in 0.1 M potassium phosphate/1 mM EDTA (pH 7.0). Decreasing the size of residue 29 or introducing Phe^{29} into the protein causes an increase in the 1932-cm^{-1} component.

cm^{-1} (Figure 5). This mutation also causes a dramatic 50-fold decrease in K_{CO} (Table 1). A preliminary crystal structure of Trp^{29} oxymyoglobin indicates that the phenyl portion of the indole ring lies on top of the bound ligand, causing a very distorted Fe–O–O geometry (T. Li and G. N. Phillips, Jr., unpublished results). This indicates substantial steric hindrance with the bound ligand and explains the low affinity constant for CO. The shifts to higher frequency may be the result of this hindrance or of interaction with the negative portion of the aromatic multipole.

Substitutions at the CD Corner and Effects of pH. The remaining amino acid that is adjacent to coordinated ligands is Phe^{43} (CD1), which is the second most highly conserved residue in myoglobins and hemoglobins. This residue plays a major role in heme binding. All naturally occurring point mutations at this position in human hemoglobin (CD1 in β-subunits and CE1 in α-subunits) give rise to unstable proteins, which readily lose the prosthetic group (Bunn & Forget, 1986). We have examined two mutations at this position, Phe^{43}→Val and Trp. The CO forms of both mutants exhibit reduced CO affinity and broad IR bands centered at significantly higher frequency than the wild-type protein (Figure 8A, Table 1). The Val^{43} protein is very unstable and exhibits heterogeneous ligand binding time courses, which precludes quantitative analysis. The increase in ν_{CO} with the decreasing size of residue 43 is probably due to increased disorder in the distal pocket, allowing movement of His^{64} away from bound CO. In the case of the Trp^{43} mutant, the large side chain at residue 43 probably pushes His^{64} away from the bound ligand as well as sterically hinders access to the iron atom.

The pH dependence of CO binding and the stretching frequency of the bound ligand have been studied intensively for over 30 years (Shimada & Caughey, 1982; Doster et al., 1982; Coletta et al., 1985; Ansari et al., 1987; Ramsden & Spiro, 1989; Morikis et al., 1989; Tian et al., 1993). When native CO–myoglobin is acidified (pH ≤ 5.0), there is extensive conversion to the A_0 (CO band at 1960 cm^{-1} and Fe–C band at 490 cm^{-1}) conformer and a marked increase in the rate of CO binding. The A_0 and A_1 conformers have been assigned to CO–myoglobins containing the distal histidine in "open" and "closed" conformations, respectively (Morikis et al., 1989). Dramatic increases in both CO association and dissociation rate constants have been observed for myoglobin in the open conformation (Tian et al., 1993). These changes have been interpreted as due to protonation of the distal histidine, which causes the imidazole side chain to swing out toward the solvent phase. Yang and Phillips (F. Yang and G. N. Phillips, Jr., manuscript in preparation) have recently confirmed that the His^{64} side chain does adopt the open conformation when $P2_1$ crystals of native CO–myoglobin are soaked in buffer at pH 4.0 [also see Quillin et al. (1992)]. Consistent with the resonance Raman data of Zhu et al. (1992), protonation of the proximal histidine and disruption of the Fe–His^{93} bond were not observed for CO–myoglobin in $P2_1$ crystals at pH 4.0. This change from the closed to the open conformation should alleviate any steric hindrance and disrupt hydrogen bonding with the bound ligand, both of which could account for the increase in ν_{CO}. Unfortunately, these interpretations are still potentially complicated by protonation of the proximal histidine, which occurs at lower pH values (Giacometti et al., 1977; Coletta et al., 1985; Sage et al., 1991a,b). Sage et al. (1991a,b) have observed a significant amount of protonation of the proximal histidine and unfolding of myoglobin in solutions at pH ≤ 4.0.

The Arg^{45}→Glu mutation was constructed to increase the pK_a of the distal histidine, so that the effects of protonation of this residue could be observed at higher pH values where complications due to the proximal histidine or myoglobin unfolding would not occur. The preliminary crystal structure of Glu^{45} myoglobin reveals disruption of the hydrogen-bonding network, which occurs in the wild-type protein between Arg^{45}, the heme 6-propionate, solvent water molecules, and His^{64} (T. Li, F. Yang, and G. N. Phillips, Jr., unpublished results). The side chain of Glu^{45} is completely disordered and cannot be located in the electron density map. We have previously shown that a similar mutation in pig myoglobin, Lys^{45}→Glu, causes a marked increase in the pH dependence of k'_{CO} in the 7.0–5.0 range (Brantley et al., 1993). At neutral pH, Glu^{45} sperm whale CO–myoglobin shows a small, but significant, band centered at 1965 cm^{-1}, and lowering the pH to 5.5 increases the intensity of this A_0 band to about 50% of the total (Figure 8). In contrast, little change is observed in the IR spectrum of wild-type CO–myoglobin in this range.

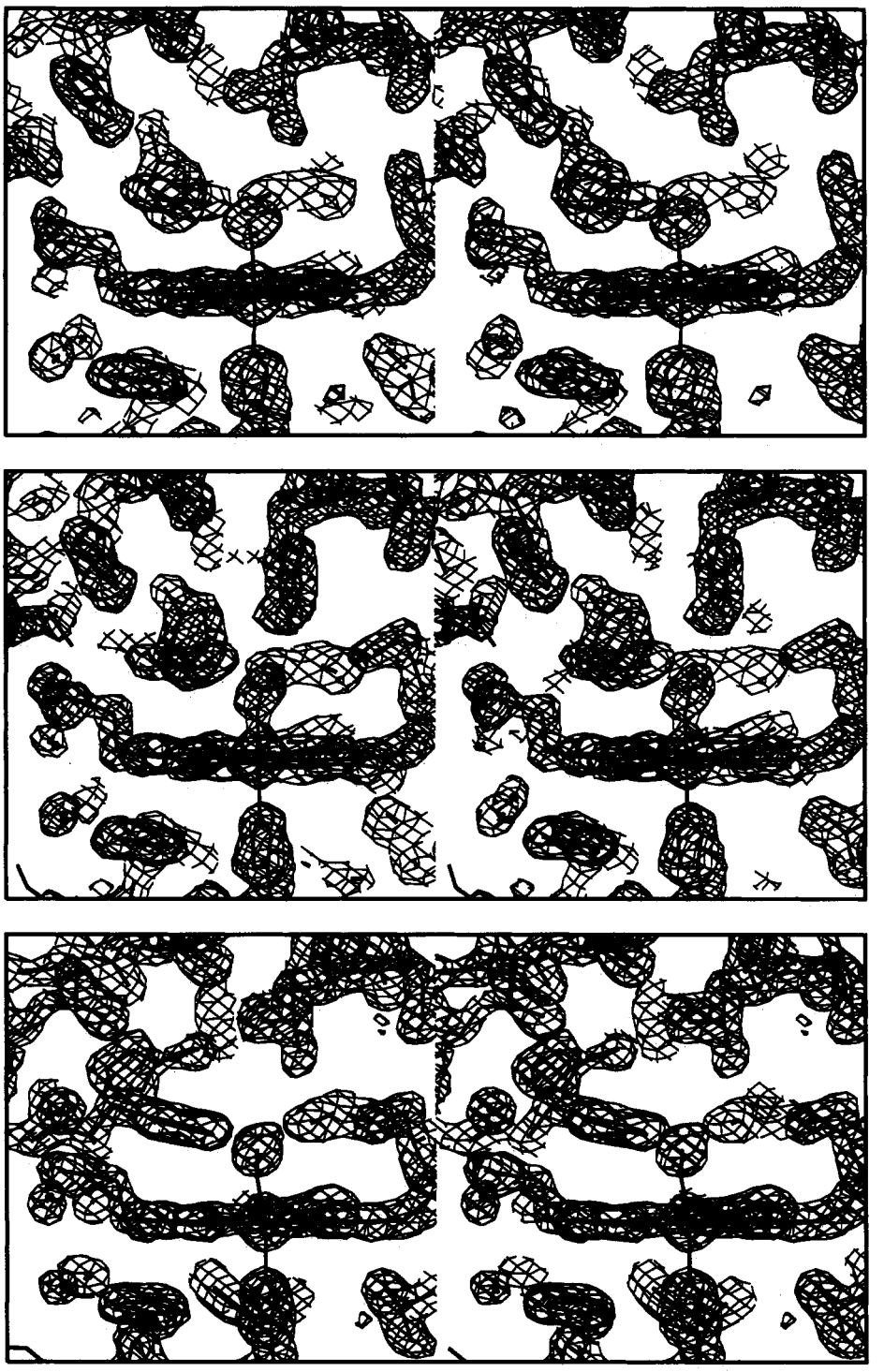

FIGURE 6: Structures of wild-type, Phe[29], and Val[46] CO–myoglobin in the P6 crystal form. From top to bottom: Stereo drawings of the electron density ($2F_o - F_c$) in the distal pockets of wild-type, Phe[29], and Val[46] CO–myoglobins, respectively. The views are from the Val[68](E11) position looking across the distal pocket toward the bound ligand and Phe[43](CD1), which is located just behind His[64]. The heme group is perpendicular to the page. Residue 64 is just to the left of the bound ligand. The solvent interface, heme 6-propionate, and Arg[45] are on the left, the proximal His[93] is at the bottom center, and residue 29 is in the upper right of each panel. For Phe[29] CO–myoglobin (middle panel), the CO ligand is located next to the edge of the phenyl ring. For Val[46] CO–myoglobin (bottom panel), the distal histidine has swung away from the bound ligand into the space created by the decrease in size of residue 46.

Key Role of Residue Phe[46](CD4). Phe[46](CD4) is highly conserved in myoglobins and hemoglobins and has been implicated in stabilizing the down conformation of the distal histidine. We have systematically varied the size of this residue from Ala to Trp and found that some of the mutations at this position markedly affect the kinetics of ligand binding to myoglobin (H. Lai, D. Lyons, T. Li, G. N. Phillips, and J. S. Olson, manuscript in preparation). Infrared spectra for the complete set of CO complexes are shown in Figure 8, and the corresponding spectral and kinetic parameters for pH 7 are listed in Table 1.

Replacement of Phe[46] with smaller amino acids (i.e., Ala, Val, Leu, and Ile) causes the appearance of a broad IR band at 1965 cm^{-1} that accounts for more than 70% of the absorbance intensity. In contrast, little change in peak position is observed for the Tyr[46] and Trp[46] substitutions. Decreasing the pH to 5.5 causes complete conversion to the high-frequency band for the mutants with aliphatic residues at position 46

Table 3: Correlation between ν_{CO}, FeCO Geometry, and the Position of the His^{64} Side Chain in Sperm Whale CO-Myoglobin Structures

protein	$\bar{\nu}_{CO}$ (cm^{-1})	FeCO angles (deg)			His^{64}–CO distances (Å)	
		Fe–C–O (θ)[a]	C–Fe–N_A	OC–Fe–N_A (ϕ)[a]	N_ϵ→C	N_ϵ→O
wild-type (Leu^{29}–Phe^{46}–His^{64}–Val^{68})	1941	169	93	224	3.5	3.1
Phe^{29}	1932	157	92	165	3.5	3.0
Val^{46}	1962	162	89	170	6.9	6.4
Ala^{68} [b]	1943	172	96	216	2.9	2.5
Phe^{68} [b]	1940	162	88	179	2.9	2.5
pig Thr^{68} [c]	1958	162(A)	95(A)	216(A)	3.0(A)	2.8(A)
		163(B)	90(B)	179(B)	3.2(B)	2.9(B)
Gln^{64} [d]	1945	171	89	173	3.4[e]	3.1[f]
Gly^{64} [d]	1965	159	89	205		
Leu^{64} [d]	1966	156	84	205		

[a] The estimated standard deviations for θ and ϕ were ±10° and 20°, respectively. [b] M. L. Quillin and G. N. Phillips, Jr., unpublished results. [c] Cameron et al. (1993). [d] Quillin et al. (1993). [e] The distance shown is from the N_ϵ atom of Gln^{64} to the C atom of the bound CO. [f] The distance shown is from O_ϵ atom of Gln^{64} to the O atom of the bound CO.

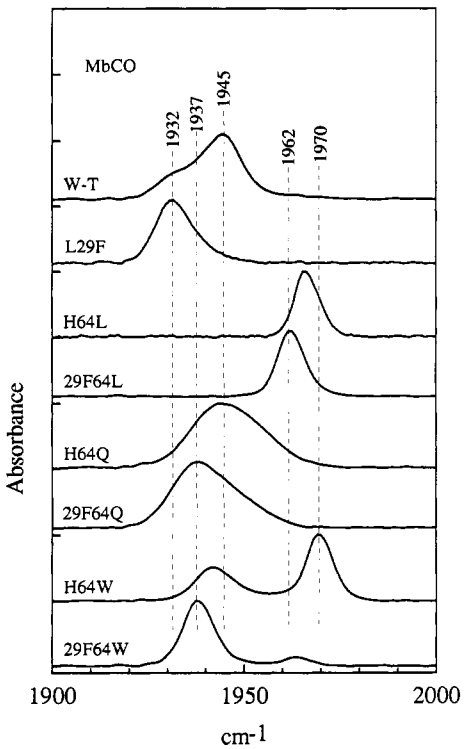

FIGURE 7: IR spectra of position 29 and 64 mutants of sperm whale CO-myoglobin measured at room temperature (~22 °C) in 0.1 M potassium phosphate/1 mM EDTA (pH 7.0). The double mutants Phe^{29}Leu^{64}, Phe^{29}Gln^{64}, and Phe^{29}Trp^{64} are listed as 29F64L, 29F64Q, and 29F64W, respectively. In all of the double mutants examined, the mutation Leu^{29}→Phe causes a decrease in ν_{CO}.

and the appearance of strong 1968-cm^{-1} bands for the Tyr^{46} and Trp^{46} mutants.

The distal histidine is disordered in the aquomet structures of the Val^{46} and Leu^{46} mutants, even though a water molecule is coordinated to the iron atom (Lai et al., manuscript in preparation). The structure of Val^{46} CO-myoglobin is shown in Figure 6 (bottom panel). Significant perturbations of the CD corner and E-helix are observed. His^{64} rotates about the C_α–C_β bond, partially filling the space occupied by the Phe^{46} side chain in the native protein. The refined occupancy of the imidazole ring in this out position is 77%. To make room for the distal histidine, the side chain of Arg^{45} extends out into the solvent with a refined occupancy of 60%. This open configuration is analogous to that seen when large ligands bind to native myoglobin or that at low pH when the distal histidine is protonated (Ringe et al., 1984; Johnson et al., 1989; Quillin et al., 1992; Yang & Phillips, manuscript in preparation).

The geometry of the ligand complex is little affected by the protein conformational changes in the Val^{46} mutant, and the Fe–C–O angle is still not linear (θ = 162°, Table 3). In addition, the affinities of the Ala^{46}, Val^{46}, Ile^{46}, and Leu^{46} mutants for CO are all 2–3-fold smaller than that for the wild-type protein. The decreases in K_{CO} for these position 46 mutants are caused mainly by significant increases in rates of CO dissociation (Table 1). These results imply that steric hindrance by the distal histidine is not the major cause of the slightly bent CO geometry. The small decreases in K_{CO} suggest that His^{64} may actually be stabilizing the bound ligand by electrostatic interactions. The increase in ν_{CO} observed for the aliphatic mutations at position 46 is readily explained by movement of His^{64} away from the bound ligand, disrupting these polar interactions with the bound ligand.

DISCUSSION

Structural Interpretations of the Vibrational Conformers. Starting with Caughey's original work, a variety of models have been proposed to explain the bands observed in the IR spectrum of bound CO (Maxwell & Caughey, 1976; Frauenfelder et al., 1988; Park et al., 1991; Li & Spiro, 1988). In all of the theories, a redistribution of resonance structures is proposed to account for the differences in the order of the Fe–C and C–O bonds. Over 30 years ago, Pauling (1960) considered the structure of gaseous CO in terms of three resonance forms: $^-C{\equiv}O^+$ (50%) ↔ C=O (40%) ↔ $^+C{=}O^-$ (10%). A similar, but more complex, set of resonance forms applies to Fe–carbonyl complexes, depending on the degree of back-bonding form the iron atom. Three possible structures are sketched below and represent a summary of the ideas presented by Caughey, Spiro, Oldfield, and co-workers (Maxwell & Caughey, 1976; Park et al., 1991; Ray et al., 1993):

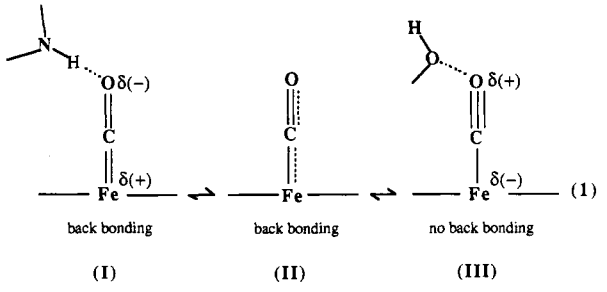

The high-frequency component (A_0) represents a mixture of mostly forms II and III, and the low-frequency components (A_1–A_3) represent more uniform mixtures of I and II. A complete molecular orbital analysis analogous to that of

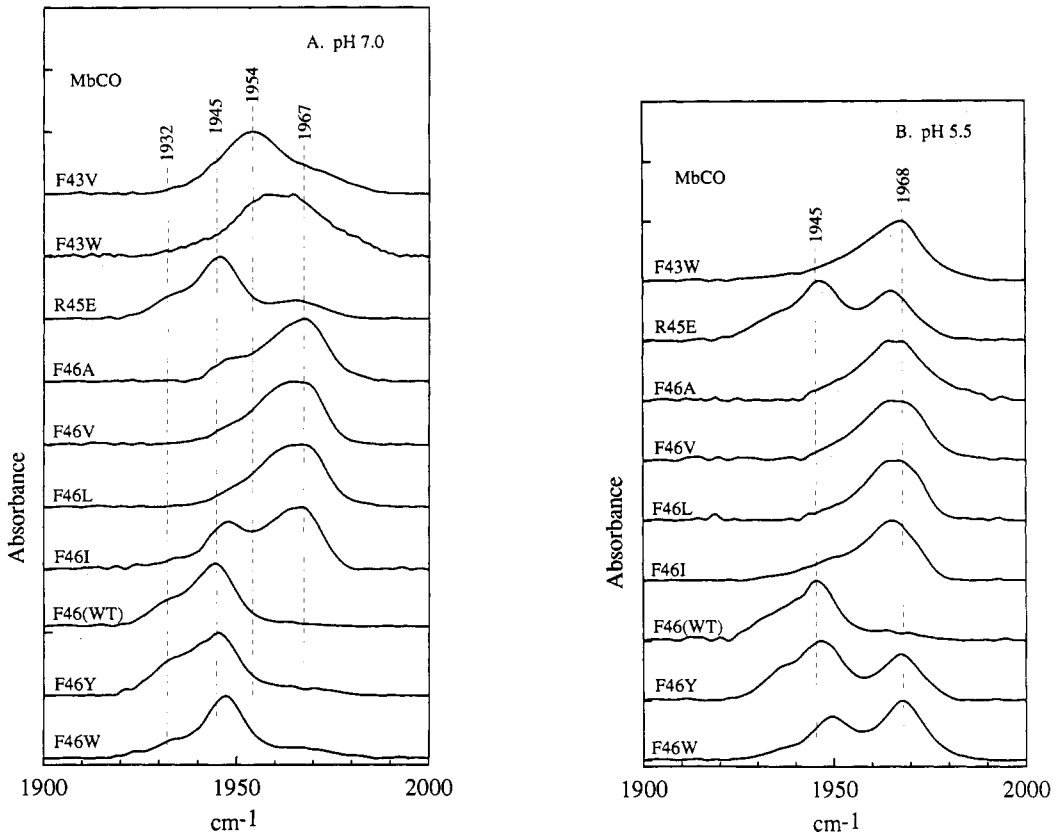

FIGURE 8: IR spectra of position 43, 45, and 46 mutants of sperm whale CO–myoglobin measured at room temperature (~22 °C) in 0.1 M potassium phosphate/1 mM EDTA: (A) pH 7.0 samples; (B) pH 5.5 samples. The spectra of position 43, 45, and 46 mutants exhibit greater amounts of high-frequency bands than does wild-type CO–myoglobin at either pH.

Hoffman et al. (1977), Li and Spiro (1988), and Park et al. (1991) is needed for a quantitative interpretation.

Lack of Correlation between CO Affinity and Fe–C–O Geometry. The resonance forms in eq 1 imply a linear Fe–C–O complex, which is generally accepted as the most stable geometry. Virtually all model CO–heme compounds exhibit an Fe–C–O angle (θ) equal to 180° (Li & Spiro, 1988). However, the values of θ reported for all known Co–myoglobin structures are significantly smaller, ranging from 170–160° in the *P*6 crystal form to 140–120° in the $P2_1$ form [Table 3; see also Kuryan et al. (1986)]. These deviations from linearity have been used as evidence that the Fe–C–O complex is severely hindered in the protein since the energies required for distortion are thought to be very large [see Ray et al. (1993)]. On the other hand, Hoffman et al. (1977) have argued that some degree of bending of the Fe–C–O moiety can occur if there is an optimal match in energy and good overlap between the π^* orbital of CO and the z^2 orbital of the iron.

The question of the magnitude of distortion energies cannot be resolved by the crystallographic data in Table 3 due to the large errors inherent in θ and ϕ angle determinations in the proteins. However, the combination of results in Tables 1–3 does suggest that small amounts of bending or distortion of the Fe–C–O complex from linearity may not play a significant role in regulating CO affinity, at least in myoglobin. First, all of the recombinant myoglobins show $\theta \approx 160$–170° in the *P*6 crystal form, despite a wide range of CO affinities (Table 3; Quillin et al., 1993). Second, the IR spectrum of crushed *P*6 crystal suspensions of wild-type CO–myoglobin is identical to that of the spectrum measured for solutions (T. Li and J. S. Olson, unpublished results), implying that the structure of the distal pocket is not perturbed significantly by crystallization. Third, the affinity of Leu^{64} myoglobin for CO is approximately equal to that of sterically unhindered model hemes, even though the Fe–C–O angle is ~160° and clearly not linear, based on inspection of the electron density maps (Quillin et al., 1993). Fourth, a bent Fe–C–O geometry is still observed when steric hindrance with His^{64} and Val^{68} has been removed by replacing these amino acids with smaller residues or by allowing the distal histidine to move away from the bound ligand (structures of Gly^{64}, Ala^{68}, Gly^{64}Ala^{68}, and Val^{46} CO–myoglobin, Figure 6; Quillin et al., 1993; Braunstein et al., 1988).

Electrostatic Effects. The key feature of eq 1 is that positive electrostatic potentials near the second ligand atom promote the formation of resonance structures with lower C–O and higher Fe–C bond orders. This accounts for the relatively low stretching frequencies and dissociation rate constants for native myoglobins containing a distal histidine and for the further decreases in k_{CO} and ν_{CO} when the N_δ atom of Asn^{68} and the positive edge of the Phe^{29} multipole are present near the second bound ligand atom (Table 1). This phenomenon has also been observed in model compounds, in which pivaloylamide N atoms can donate a proton to bound CO, and in cytochrome *c* and horseradish peroxidase, where the distal pockets contain both a histidine and an arginine (Li & Spiro, 1988; Ray et al., 1993). Removal of proton donors or the addition of partial negative charge in the distal pocket has the opposite effect and promotes the formation of more of the $^-Fe—C{\equiv}O^+$ resonance structure. This accounts for the increase in both ν_{CO} and k_{CO} when His^{64} is replaced by apolar amino acids, when the imidazole side chain rotates away from the bound ligand in the Val^{46} mutant or at low pH, and when hydroxyl groups are introduced into the position 68 side chain (Tables 1 and 2).

One of the most dramatic shifts in stretching frequency is observed for the $Fe^{II}C_2Cap(NMeIM)(CO)$ model compound

[5,10,15,20-tetrakis(pyromellitoyl-*o*-(oxyethoxy)phenyl)porphyrinatoiron(II)], which has a ν_{CO} peak at 2002 cm^{-1} compared to 1966–1970 cm^{-1} for the uncapped precursor (Ray et al., 1993). The C_2Cap heme has a benzene ring cap located directly above the bound CO ligand. As pointed out by Ray et al. (1993), this places the negative center of the aromatic multipole directly above the second ligand atom, stabilizing the triple-bonded CO resonance structure (III in eq 1) and increasing ν_{CO} dramatically.

Equation 1 also provides an interpretation of the line-broadening effects observed for mutants in which the distal pocket cavity is made larger and more accessible to solvent. Interactions with water molecules should stabilize the partially charged resonance forms, causing both increases and decreases in ν_{CO}. This is particularly dramatic in the His^{64}→Gly, Ala and Phe^{46}→Ala, Val, Ile, and Leu mutants. In the case of the Leu^{29}→Ala, Val, and Ile mutants, there is more room for a solvent water molecule next to the bound ligand in the interior of the pocket. Since the iron–carbonyl is already polarized by His^{64}, extra solvent water is likely to act as a proton donor. This would enhance the population of structures I and II by further stabilizing partial negative charge on the oxygen atom of bound CO. This would account for the increase in intensity of the 1932 cm^{-1} band for Ala^{29}, Val^{29}, and Ile^{29} myoglobin (Figure 5). These solvent interactions are transient and not well-ordered since no discrete electron density peaks attributable to water have been found in the distal pockets of any of the CO–myoglobin structures reported in Table 3. However, an extra, non-coordinated water molecule is found at 80% occupancy in the back of the distal pocket of wild-type metmyoglobin and Gly^{64} CO–myoglobin (Quillin et al., 1993), and transient water molecules are expected to be present near the ligand binding site on the basis of the molecular dynamics simulations of Lounnas and Pettitt (V. Lounnas and B. M. Pettitt, manuscript in preparation). In the absence of a large side chain at position 64, these distal pocket water molecules act as proton donors and bases intermitantly, placing positive and negative charges adjacent to the bound CO. The net effect is a broadening of the IR CO bands of Gly^{64} and Ala^{64} CO–myoglobins.

Neutron diffraction studies of native CO–myoglobin in the $P2_1$ crystal form show that, in contrast to the oxy complex, there appears to be no deuterium atom on the N_ϵ atom of the imidazole side chain adjacent to the ligand atom; instead, it appears attached to N_δ (Hanson & Schoenborn, 1981; Cheng & Schoenborn, 1991). This suggests that there is no hydrogen bond to the bound CO, despite the low value of ν_{CO}. Several arguments have been proposed to account for this discrepancy: (1) the imidazole tautomer equilibrium is shifted by dehydration in the $P2_1$ crystals (Lian et al., 1993); (2) crystal packing constraints distort the geometry of the bound ligand and the distal histidine (Quillin et al., 1993); and (3) stabilization of an sp^2 conformer occurs through direct interaction between the nonbonded electrons on the N_ϵ atom and the positively charged carbon atom (Ray et al., 1993; Maxwell & Caughey, 1976). A combination of these effects may occur, but, in fact, there is not a serious discrepancy. The neutral resonance structure (II) must be the dominant form since the observed CO stretching frequencies (1900–2000 cm^{-1}) are between the values for simple carbonyls (~1750 cm^{-1}) and triple-bonded structures (~2200 cm^{-1}). Only a small fraction of N_ϵ–H tautomer is needed to promote the formation of a slight increase in resonance structure I and a resultant decrease in ν_{CO}. Regardless of the exact interpretation, electrostatic interactions between bound CO and the distal histidine are weak, at least when compared to the interactions with the Fe–O–O complex where disruption of hydrogen bonding results in 100–1000-fold increases in the overall rate constant for oxygen dissociation. Thus, other effects such as crystal packing and hydration probably exert a greater influence on the tautomer structure of His^{64} than does bound CO.

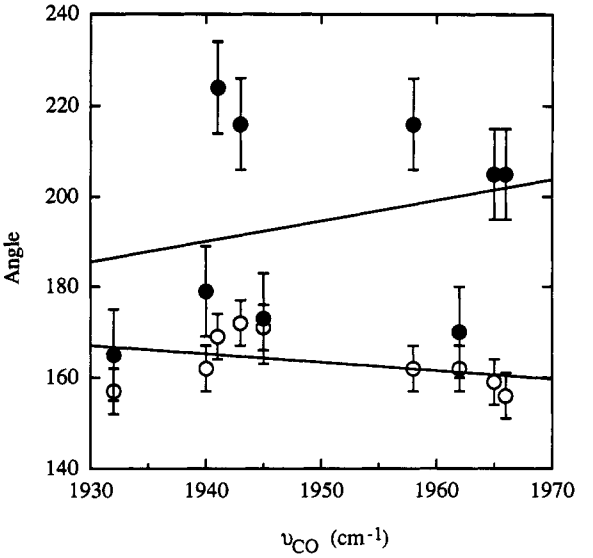

FIGURE 9: Plots of the $\bar{\nu}_{CO}$ (cm^{-1}) values *versus* the Fe–C–O (θ) (○) and OC–Fe–N_A (ϕ) (●) angles. Estimated standard deviations for θ and ϕ of the CO–myoglobins are 10° and 20°, respectively. The data were taken from Table 3. The straight lines are from linear least-squares fits to the observed data points, and the correlation coefficients are 0.3 and 0.2, respectively, for the plot of Fe–C–O (θ) *versus* $\bar{\nu}_{CO}$ and that of OC–Fe–N_A (ϕ) *versus* $\bar{\nu}_{CO}$. Thus, there is no apparent correlation between the Fe–C–O (θ) or OC–Fe–N_A (ϕ) angle and $\bar{\nu}_{CO}$.

Structural Interpretation of the A States. The spectra in Figures 2–5, 7, and 8 indicate that a continuum of states is allowed for the heme–Fe–C–O complex, with ν_{CO} ranging from ~1900 to ~2000 cm^{-1} [see also Ray et al. (1993)]. In contrast, there is little variation in the Fe–C–O angle between the nine structures of recombinant myoglobins, which have been determined by X-ray crystallography. As shown in Figure 9 and Table 3, there is no correlation between ν_{CO} and any of the bond angles for the iron–ligand complexes. Since the error in the Fe–C–O angle (θ) is estimated to be ±10°, it is difficult to judge the experimental significance of the differences between the various mutants. The crystallographic results do show that the appearance of 1930–1940-cm^{-1} bands requires the presence of a nitrogen atom within hydrogen-bonding distance of the second bound ligand atom (Table 3, columns 6 and 7).

The assignment of A substates to specific resonance structures in eq 1 is difficult. Even at cryogenic temperatures interconversion of the resonance forms should be extremely rapid. As pointed out by Frauenfelder and co-workers (Frauenfelder et al., 1988), the differential rates of geminate rebinding to the A_0, A_1, and A_3 substates are a reflection of small differences in the orientation of key distal pocket residues, which are frozen in place at 10–100 K. Thus, the A_0 substate in native myoglobin probably represents a set of conformations in which the His^{64} side chain has rotated far enough away from the bound ligand to reduce electrostatic interactions. Since the imidazole ring is no longer immediately adjacent to the iron atom and is fixed in position at these extremely low temperatures, CO rebinding should be very fast. In the A_3 substate, His^{64} is interacting strongly with bound CO, and its proximity to the iron atom should sterically hinder geminate rebinding.

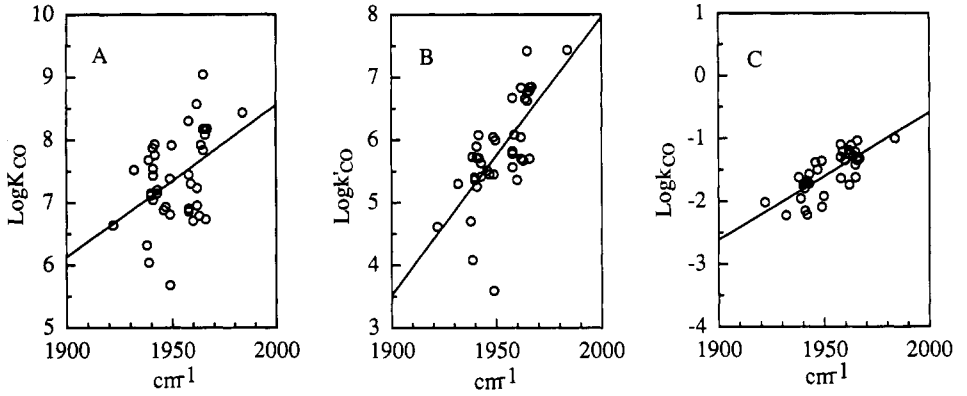

FIGURE 10: Correlation between rate and equilibrium constants for CO binding and $\bar{\nu}_{CO}$ for sperm whale and pig myoglobin mutants: (A) plot of log(K_{CO}) *versus* $\bar{\nu}_{CO}$ (cm^{-1}); (B) plot of log(k'_{CO}) *versus* $\bar{\nu}_{CO}$ (cm^{-1}); (C) plot of the log(k_{CO}) *versus* $\bar{\nu}_{CO}$ (cm^{-1}). The data were taken from Tables 1 and 2. The straight lines are from linear least-squares fits to the observed data points, and the correlation coefficients are 0.4, 0.7, and 0.8, respectively, from the plot of the log(K_{CO}) *versus* $\bar{\nu}_{CO}$, that of log(k'_{CO}) *versus* $\bar{\nu}_{CO}$, and that of log(k_{CO}) *versus* $\bar{\nu}_{CO}$. Thus, there is little significant correlation between K_{CO} and $\bar{\nu}_{CO}$. In contrast, increases in k_{CO} do correlate with increases in ν_{CO}, and intermediate results were obtained with k'_{CO} and $\bar{\nu}_{CO}$.

As shown in Table 3 and Figure 9, the Fe–C–O angles determined by X-ray crystallography do not reveal any correlation with the A substates. For example, the Fe–C–O angles of Gly^{64}, Leu^{64}, and Val^{46} CO–myoglobins, which display mostly A_0 conformer, are identical within experimental error to that of Phe^{29} CO–myoglobin, which contains mostly A_3 conformer. This again indicates that protein conformers, and not different Fe–C–O angles, cause the variation in ν_{CO} (Frauenfelder et al., 1988; Moore et al., 1988). A more detailed structural understanding of the substates and the kinetic barriers requires low-temperature and IR linear dichroism studies with sets of distal pocket mutants, such as those listed in Tables 1 and 2 [see Carver et al. (1990), Smerdon et al. (1991), Gibson et al. (1992), Balasubramanian et al. (1993), Braunstein et al. (1993), and Mourant et al. (1993)].

Determinants of CO Affinity. The key problem in discriminating between mechanisms based on polar *versus* steric interactions is how to obtain structural and functional estimates of hindrance. On the basis of pH and position 64 mutagenesis studies, many authors have argued that the A_0 or high-frequency IR band always represents an open conformation, in which the distal histidine has either swung away from the bound ligand or been removed, both of which would relieve steric hindrance. This would explain the higher association rate and equilibrium constants for most of the position 64 mutants, the increase in k'_{CO} with decreasing pH, and the selectively higher rates of geminate recombination of the A_0 conformer at cryogenic temperatures (Frauenfelder et al., 1988). However, when a complete set of distal pocket mutants is examined, the correspondence between high-frequency IR bands and ligand reactivity breaks down (Figure 10AB). Thus, the A substate labels designate only the order of the C–O bond and not necessarily the degree of hindrance in the distal pocket.

As shown in Figure 10A, there is very little, if any, correlation between ν_{CO} and K_{CO}. The simplest explanation of the results in Figure 10A is that the relative population of resonance structures and, thus, ν_{CO} is governed primarily by electrostatic potentials and is little influenced by steric hindrance. In contrast, CO affinity is determined by a complex set of effects, which include the following: (1) inhibitory polar interactions that stabilize water molecules in the distal pocket of deoxymyoglobin; (2) steric hindrance that blocks access to the iron atom and creates strain on the bound ligand; (3) favorable hydrogen bonding or positive electrostatic potentials that enhance back-bonding and increase the order of the Fe–C bond; and (4) unfavorable negative electrostatic potentials, which decrease back-bonding and the Fe–C bond order. In the case of CO binding, effects 3 and 4 are small because of the inherent neutrality of the CO complex (form II, eq 1). Li and Spiro (1988) and Ray et al. (1993) have shown that the energies associated with polarization of the Fe–C–O bonds and the consequent changes in ν_{CO} are small compared with those associated with bending distortions. Thus, the dominant factors governing CO affinity in myoglobin appear to be water displacement from the distal pocket and direct steric hindrance.

Inhibition due to polar and steric interactions in deoxymyoglobin should be exerted primarily on the overall association rate constants, k'_{CO}, since distal pocket water and/or hindering side chains must be displaced before the ligand can bind. An exact interpretation depends on the rate-limiting step for association, which is determined by the intrinsic reactivity of the ligand with iron [see Carver et al. (1990) and Gibson et al. (1992)]. The last two electrostatic effects should be exerted primarily on the overall dissociation rate constant, k_{CO}, which in the case of CO is governed primarily by the thermal rate of Fe–C bond breakage and is little affected by geminate rebinding processes. This accounts for the correlation between k_{CO} and ν_{CO}, since both the order of the C–O bond and the rate of dissociation are inversely related to the strength of the Fe–C bond (Figure 10C; Uno et al., 1985).

The lack of correlation between K_{CO} and ν_{CO} (Figure 10A) is readily explained by the requirement of water displacement from the distal pocket when His^{64} is present and by the insensitivity of the Fe–C–O bond orders to steric hindrance. For example, the Val^{68}→Asn and Thr mutations both decrease K_{CO}, whereas these substitutions produce opposite effects on ν_{CO} (Tables 1 and 2 and Figures 3 and 4). Both side chains can stabilize the non-coordinated water, which is hydrogen-bonded to the distal histidine in deoxymyoglobin (Quillin et al., 1993; Cameron et al., 1993). In the case of Thr^{68}, and β-hydroxyl accepts a proton from the distal pocket water molecule, whereas the Asn^{68} amide nitrogen may donate a proton to the water oxygen atom. These extra hydrogen-bonding interactions must be disrupted before a ligand molecule can coordinate to the iron atom and, thus, even though the electrostatic potentials exerted on the bound ligand are of opposite sign, both mutations cause a decrease in affinity.

Some hydrogen bonding is also likely to occur between the bound ligand and the amide N_δ of Asn^{68}. The resultant positive electrostatic potential should decrease the order of the C–O bond and increase the order of the Fe–C bond, accounting for the ~20-cm^{-1} decrease in ν_{CO} and 2-fold

decrease in k_{CO} compared to the corresponding wild-type parameters (Table 1). In the Thr[68] mutant, the partial negative charge on the hydroxyl group increases the order of the C–O bond and decreases the order of the Fe–C bond, causing an 18-cm^{-1} increase in ν_{CO} and a 4-fold increase in k_{CO} (Table 2). Steric hindrance plays a dominant role in reducing CO affinity for the Ile[68] and Trp[29] mutants, due to the proximity of the larger side chains to the ligand binding site. As a result, both the association rate and equilibrium constants for CO binding to these mutants are reduced markedly compared to wild-type protein, but only small changes in k_{CO} and ν_{CO} are observed. Similar arguments can be made to explain the rate and equilibrium constants of the remaining mutants in Tables 1 and 2 and, thus, electrostatic interactions with the Fe–C–O resonance structures shown in eq 1 provide a self-consistent interpretation of all of the stretching frequency data.

Conclusion. The IR spectra, rate and equilibrium constants, and structures presented here, coupled with the survey of model compounds and other heme proteins described by Ray et al. (1993), provide convincing evidence that the vibrational spectrum of CO bound to myoglobin is a sensitive gauge of surrounding electrostatic potentials. In contrast, the bond orders and geometry of the Fe–C–O complex are relatively insensitive to steric hindrance. Thus, the A substates assigned to peak intensities in the IR spectrum of CO–myoglobin reflect the sign and strength of the electrostatic potential vector in the vicinity of the binding site and not necessarily sterically constrained or unhindered conformations.

ACKNOWLEDGMENT

We thank Eileen Singleton for expressing and purifying the sperm whale myoglobin mutants and constructing new mutants as the work progressed; Cynthia Li for preparing all of the pig myoglobin samples at Rice University and Anthony Wilkinson for supplying the plasmids for these proteins; Henry Lai and Daniel Lyon for sharing their results for the position 46 mutants; and Tim Whitaker for constructing the Trp[43] mutant. Professor George Schroepfer, Jr., and Dr. William Wilson very graciously allowed us to use their IR spectrometer and provided valuable help and encouragement. Finally, we are indebted to Dr. Thomas G. Spiro for carefully reading the original manuscript and suggesting several key improvements in the Discussion section.

REFERENCES

Adachi, S.; Sunohara, N.; Ishimori, K., & Morishima, I. (1992) *J. Biol. Chem. 267*, 12614–12621.

Alben, J. O., & Caughey, W. S. (1968) *Biochemistry 7*, 175–183.

Ansari, A.; Berendzen, J.; Braunstein, D., Cowen, B. R., Frauenfelder, H., Hong, M. K., Iben, E. T., Johnson, J. B., Ormos, P., Sauke, T. B., Scholl, R., Schulte, A., Steinbach, P. J., Vittitow, J., & Young, R. D. (1987) *Biophys. Chem. 26*, 337–355.

Balasubramanian, S., Lambright, D. G., & Boxer, S. G. (1993) *Proc. Natl. Acad. Sci. U.S.A. 90*, 4718–4722.

Brantley, R. E., Jr., Smerdon, S. J., Wilkinson, A. J., Singleton, E. W., & Olson, J. S. (1993) *J. Biol. Chem. 268*, 6995–7010.

Braunstein, D. P., Ansari, A., Berendzen, J., Cowen, B. R., Egeberg, K. D., Frauenfelder, H., Hong, M. K., Ormos, P., Sauke, T. B., Scholl, R., Schulte, A., Sligar, S. G., Springer, B. A., Steinbach, P. J., & Young, R. D. (1988) *Proc. Natl. Acad. Sci. U.S.A. 85*, 8497–8501.

Braunstein, D. P., Chu, K., Egeberg, K. D., Frauenfelder, H., Mourant, J. R., Nienhaus, G. U., Ormos, P., Sligar, S. G., Springer, B. A., & Young, R. D. (1993) *Biophys. J. 65*, 2447–2454.

Brunger, A., Karplus, M., & Petsko, G. A. (1989) *Acta Crystallogr. 45*, 50–61.

Bunn, H. F., & Forget, B. G. (1986) *Hemoglobin: Molecular, Genetic and Clinical Aspects*, pp 565–594, W. B. Saunders Company, Philadelphia.

Cameron, A. D., Smerdon, S. J., Wilkinson, A. J., Habash, J.; Helliwell, J. R., Li, T., & Olson, J. S. (1993) *Biochemistry 32*, 13061–13070.

Carver, T. E., Rohlfs, R. J., Olson, J. S., Gibson, Q. H., Blackmore, R. S., Springer, B. A., & Sligar, S. G. (1990) *J. Biol. Chem. 265*, 20007–20020.

Carver, T. E., Brantley, R. E., Singleton, E. W., Arduini, R. M., Quillin, M. L., Phillips, G. N., Jr., & Olson, J. S. (1992) *J. Biol. Chem. 265*, 14443–14450.

Caughey, W. S., Alben, J. O., McCoy, S., Boyer, S. H., Carache, S., & Hathaway, P. (1969) *Biochemistry 8*, 59–62.

Caughey, W. S., Shimada, H., Miles, G. C., & Tucker, M. P. (1981) *Proc. Natl. Acad. Sci. U.S.A. 78*, 2903–2907.

Cheng, X., & Schoenborn, B. P. (1991) *J. Mol. Biol. 220*, 381–399.

Choc, M. G., & Caughey, W. S. (1981) *J. Biol. Chem. 256*, 1831–1838.

Coletta, M., Ascenzi, P., Traylor, T. G., & Brunori, M. (1985) *J. Biol. Chem. 260*, 4151–4155.

Collman, J. P., Brauman, J. I., Halbert, T. R., & Suslick, K. S. (1976) *Proc. Natl. Acad. Sci. U.S.A. 73*, 333–3337.

Egeberg, K. D., Springer, B. A., Martinis, S. A., Sligar, S. G., Morikis, D., & Champion, P. M. (1990a) *Biochemistry 29*, 9783–9791.

Egeberg, K. D., Springer, B. A., Sligar, S. G., Carver, T. E., Rohlfs, R. J., & Olson, J. S. (1990b) *J. Biol. Chem. 265*, 11788–11795.

Finzel, B. C. (1987) *J. Appl. Crystallogr. 20*, 53–55.

Frauenfelder, H., Park, F., & Young, R. D. (1988) *Annu. Rev. Biophys. Chem. 17*, 451–479.

Giacometti, G. M., Traylor, T. G., Ascenzi, P., Brunori, M., & Antonni, E. (1977) *J. Biol. Chem. 252*, 7447–7448.

Gibson, Q. H., Regan, R., Elber, R., Olson, J. S., & Carver, T. E. (1992) *J. Biol. Chem. 267*, 22022–22034.

Hanson, J. C., & Shoenborn, B. P. (1981) *J. Mol. Biol. 153*, 117–146.

Hoffman, R., Chen, M. M.-L., & Thorn, D. L. (1977) *Inorg. Chem. 16*, 503–511.

Ikeda-Saito, M., Hori, H., Anderson, L. A., Prince, R. C., Pickering, I. J., George, G. N., Saunders, C. R., II, Lutz, R. S., McKelvey, E. J., & Maltera, R. (1992) *J. Biol. Chem. 267*, 22843–22852.

Johnson, K. A., Olson, J. S., & Phillips, G. N., Jr. (1989) *J. Mol. Biol. 207*, 459–463.

Kabsch, W. (1988) *J. Appl. Crystallogr. 21*, 916–924.

Kim, K., & Ibers, J. (1991) *J. Am. Chem. Soc. 113*, 6077–6081.

Kraulis, P. J. (1991) *Appl. Crystallogr. 24*, 946–950.

Kunkel, T. A. (1985) *Proc. Natl. Acad. Sci. U.S.A. 82*, 488–493.

Kuryan, J., Wilz, S., Karplus, M., & Petsko, G. A. (1986) *J. Mol. Biol. 192*, 133–154.

Li, X. Y., & Spiro, T. G. (1988) *J. Am. Chem. Soc. 110*, 6024–6033.

Lian, T., Locke, B., Kitagawa, T., Nagai, M., & Hochstrasser, R. M. (1993) *Biochemistry 32*, 5809–5814.

Makinen, M. W., Houtchens, R. A., & Caughey, W. S. (1979) *Proc. Natl. Acad. Sci. U.S.A. 76*, 6042–6046.

Marks, G. S., Brien, J. F., Nakatsu, K., & McLaughlin, B. E. (1991) *Trends Pharmacol. Sci. 12*, 185–188.

Maxwell, J. C., & Caughey, W. S. (1976) *Biochemistry 15*, 388–395.

Moore, J. N., Hansen, P. A., & Hochstrasser, R. M. (1988) *Proc. Natl. Acad. Sci. U.S.A. 85*, 5062–5066.

Morikis, D., Champion, P. M., Springer, B. A., & Sligar, S. G. (1989) *Biochemistry 28*, 4791–4800.

Morikis, D., Champion, P. M., Springer, B. A., Egeberg, K. D., & Sligar, S. G. (1990) *J. Biol. Chem. 265*, 12143–12145.

Mourant, J. R., Braunstein, D. P., Chu, K., Frauenfelder, H., Nienhaus, G. U., Ormos, P., & Young, R. D. (1993) *Biophys. J.* (submitted for publication.

Nagai, M., Yoneyama, Y., & Kitagawa, T. (1991) *Biochemistry 30*, 6495–6503.

Oldfield, E., Guo, K., Augspurger, J. D., & Dykstra, C. E. (1991) *J. Am. Chem. Soc. 113*, 7537–7541.

Ormos, P., Brauenfelder, H., Hong, M. K., Lin, S. L., Sauke, T. B., & Young, R. D. (1988) *Proc. Natl. Acad. Sci. U.S.A. 85*, 8492–8496.

Park, K. D., Guo, K., Adebodun, F., Chiu, M. L., Sligar, S. G., & Oldfield, E. (1991) *Biochemistry 30*, 2333–2347.

Peng, S.-M., & Ibers, J. A. (1976) *J. Am. Chem. Soc. 98*, 8032–8066.

Perutz, M. F., Pulsinelli, P. D., & Ranney, H. M. (1972) *Nature (London) New Biol. 237*, 259–263.

Phillips, G. N., Jr., Arduini, R. M., Springer, B. A., & Sligar, S. G. (1990) *Proteins 7*, 358–365.

Quillin, M. L., Brantley, R. E., Jr., Johnson, K. A., Olson, J. S., & Phillips, G. N., Jr. (1992) *Biophys. J. 61*, A466.

Quillin, M. L., Arduini, R. M., Olson, J. S., & Phillips, G. N., Jr. (1993) *J. Mol. Biol. 234*, 140–155.

Ramsden, J., & Spiro, T. G. (1989) *Biochemistry 28*, 3125–3128.

Ray, G. B., Li, X.-Y., Ilbers, J. A., Sessler, J. L., & Spiro, T. G. (1993) *J. Am. Chem. Soc.* (submitted for publication).

Ringe, D., Petsko, G. A., Kerr, D., & Ortiz de Montellano, P. R. (1984) *Biochemistry 23*, 2–4.

Rohlfs, R. J., Mathews, A. J., Carver, T. E., Olson, J. S., Springer, B. A., Egeberg, K. D., & Sligar, S. G. (1990) *J. Biol. Chem. 265*, 3168–3176.

Sack, J. S. (1988) *J. Mol. Graphics 6*, 244–245.

Sage, J. T., Morikis, D., & Champion, P. M. (1991a) *Biochemistry 30*, 1227–1237.

Sage, J. T., Morikis, D., & Champion, P. M. (1991b) *Biochemistry 30*, 1237–1247.

Sakan, Y., Ogura, T., Kitagawa, T., Fraunfelter, F. A., Mattera, R., & Ikeda-Saito, M. (1993) *Biochemistry 32*, 5815–5824.

Sambrook, J., Fritsch, E. F., & Maniatis, T. (1989) *Molecular Cloning: A Laboratory Manual*, Cold Spring Harbor Laboratory, Cold Spring Harbor, NY.

Shimada, H., & Caughey, W. S. (1982) *J. Biol. Chem. 257*, 11893–11900.

Smerdon, S., Dodson, G., Wilkinson, A. J., Gibson, Q. H., Blackmore, R. S., Carver, T. E., & Olson, J. S. (1991) *Biochemistry 30*, 6252–6260.

Snyder, S. H., & Brecht, D. S. (1992) *Sci. Am.* May, 68–77.

Springer, B. A., & Sligar, S. G. (1987) *Proc. Natl. Acad. Sci. U.S.A. 84*, 8961–8965.

Springer, B. A., Egeberg, K. D., Sligar, S. G., Rohlfs, R. J., Mathews, A. J., & Olson, J. S. (1989) *J. Biol. Chem. 264*, 3057–3060.

Stryer, L. (1988) *Biochemistry*, 3rd ed., pp 148–149, W. H. Freeman and Company, New York.

Tian, W. D., Sage, J. T., & Champion, P. M. (1993) *J. Mol. Biol. 233*, 155–166.

Uno, T., Nishimura, Y., Makino, R., Iizuka, T., Ishimura, Y., & Tsuboi, M. (1985) *J. Biol. Chem. 260*, 2023–2026.

Varadarajan, R., Zewert, T. E., Gray, H. B., & Boxer, S. G. (1989a) *Science 243*, 69–72.

Varadarajan, R., Lambright, D. G., & Boxer, S. G. (1989b) *Biochemistry 28*, 3771–3781.

Zhu, L., Sage, J. T., Rigos, A. A., Morikis, D., & Champion, P. M. *J. Mol. Biol. 224*, 207–215.